

High-order harmonic generation from a two-dimensional band structureJian-Zhao Jin,¹ Xiang-Ru Xiao,¹ Hao Liang,¹ Mu-Xue Wang,¹ Si-Ge Chen,¹ Qihuang Gong,^{1,2} and Liang-You Peng^{1,2,*}¹*State Key Laboratory for Mesoscopic Physics and Collaborative Innovation Center of Quantum Matter, School of Physics, Peking University, Beijing 100871, China*²*Collaborative Innovation Center of Extreme Optics, Shanxi University, Taiyuan, Shanxi 030006, China*

(Received 12 March 2018; published 19 April 2018)

In the past few years, harmonic generation in solids has attracted tremendous attention. Recently, some experiments of two-dimensional (2D) monolayer or few-layer materials have been carried out. These studies demonstrated that harmonic generation in the 2D case shows a strong dependence on the laser's orientation and ellipticity, which calls for a quantitative theoretical interpretation. In this work, we carry out a systematic study on the harmonic generation from a 2D band structure based on a numerical solution to the time-dependent Schrödinger equation. By comparing with the 1D case, we find that the generation dynamics can have a significant difference due to the existence of many crossing points in the 2D band structure. In particular, the higher conduction bands can be excited step by step via these crossing points and the total contribution of the harmonic is given by the mixing of transitions between different clusters of conduction bands to the valence band. We also present the orientation dependence of the harmonic yield on the laser polarization direction.

DOI: [10.1103/PhysRevA.97.043420](https://doi.org/10.1103/PhysRevA.97.043420)**I. INTRODUCTION**

High-order harmonic generation (HHG) in the gas phase [1,2] has led to the creation of laser pulses in the attosecond timescale [3,4], which have allowed the trace and manipulation of electronic dynamics on its natural timescale [5–7]. At the same time, as a spectroscopic tool, HHG has allowed the imaging of atomic and molecular orbitals, structures, and dynamics [8–11].

For harmonic generation in the solid phase, its experimental explorations have only sprung up in the past few years, although several theoretical discussions appeared in the 1990s [12–16]. Coherent radiations with a nonperturbative character at various wavelengths have been experimentally observed from the bulk dielectrics or semiconductors driven by different laser pulses [17–22]. In addition, harmonic generation and light-induced current have been experimentally and theoretically studied in two-dimensional materials such as graphene [23–25]. On the one hand, the investigations of current and harmonic generation in solids may provide a controllable current which promises a much faster signal processing by a temporal change of the material properties [26,27]. On the other hand, HHG in solids has the potential to study or even reconstruct the band structures of the crystals [28–30].

Some of the observed phenomena of HHG in solids have distinct differences from those observed in gas. For example, the cutoff photon energy in solids scales linearly [17] with the electric field strength F_0 of the driving laser, while it scales quadratically with F_0 in the gas phase [31–33]. To account for the features of HHG in solids, many theoretical attempts have been made during the last few years. As a first step, two-band models were proposed to explain the linear

cutoff scaling, which are essentially based on an excitation from the valence band (VB) to a conduction band (CB) with a subsequent Bloch oscillation within this single conduction band due to the reflection at the Brillouin zone boundary [17,34,35]. This model attributes the harmonic generations to the *intraband* transitions within the conduction band and is able to explain the linear scaling of the cutoff energy via the Bloch oscillation. Actually, the same linear scaling law can also be explained by considering the *interband* transition between the conduction and the valence bands [36–39]. In fact, when the laser intensity is increased, higher conduction bands may be involved in harmonic generation, in which case the harmonic yield is a coherent sum over all possible intraband and interband transitions [40,41]. Despite existing differences from the gas phase case, similarities between the underlying mechanisms have been discussed, based on the semiclassical and recollision picture [29,42,43]. The important role of the dynamic Stark shift [44] of the energy bands was recently addressed to account for the experiments in the wide-gap dielectrics [26,27]. HHG in a solid by few-cycle pulses has recently been studied theoretically [45].

Although some aspects have been understood based on the above studies, high-order harmonic generation in solids is much more complicated than expected due to the complex band structures and different mechanisms that coexist and interplay with each other. Indeed, first-principle simulations based on the time-dependent density-functional theory (TDDFT) have revealed important impacts of the electronic band structure [46–48]. Detailed studies on the selection rules for harmonic generation in solids showed that the simple analysis of the dynamical symmetry of the crystal cannot always be correct [49]. Different from cases in the gas phase, the recombination of the electron in solids may happen at different sites in the lattice and thus delocalization and spatial coherence may be important, as discussed very recently [50,51]. In addition, the

*liangyou.peng@pku.edu.cn

effect of the transition dipole phase on the HHG in solid materials has been shown to be very important [52].

An apparent feature of HHG in solids is its orientation and ellipticity dependence with respect to the symmetric axis of the crystals, which have been observed in many experiments [17,18,20,21,53] and theoretically discussed recently [47,54,55]. To describe this orientation effect, one needs to discuss the high-order harmonic generation of solids in the two-dimensional framework. Also, the two-dimensional (2D) description is important to identify the differences from the 1D models, and to understand the coupling of intraband and interband dynamics due to the existence of the crossings in the 2D band structures. In the present contribution, we address these issues by a numerical solution to the time-dependent Schrödinger equation (TDSE), based on the expansions by the augmented plane wave [56]. We find excitations to higher conduction bands in a step-by-step manner via crossings in the band structure and they can lead to multiple plateaus in the spectrum [41]. Orientation effects will be also discussed and our result qualitatively agrees with recent experimental observation [53].

The rest of the paper is organized as follows. In Sec. II, we describe the theoretical methods for the simulations. In Sec. III, we present the main results, which include a comparison with the 1D model, the HHG spectra by using a different number of basis states, the HHG at different laser parameters, and a time-frequency analysis, followed by a discussion on the orientation dependence. We summarize our results in Sec. IV.

II. THEORETICAL METHODS

We intend to solve the following two-dimensional time-dependent Schrödinger equation:

$$i\hbar \frac{\partial}{\partial t} |\Psi(x, y, t)\rangle = (H_{\text{free}} + H_{\text{int}}) |\Psi(x, y, t)\rangle, \quad (1)$$

where H_{free} is the field-free Hamiltonian for the electron quasiparticle with a mass m_0 , and H_{int} is the interaction Hamiltonian between the laser and the electron of the 2D material in the velocity gauge. They are explicitly given by

$$H_{\text{free}} = \frac{\mathbf{p}^2}{2m_0} + V(x, y), \quad (2)$$

and

$$H_{\text{int}} = \frac{e}{m_0} \mathbf{A}(t) \cdot \mathbf{p}, \quad (3)$$

respectively, in which $V(x, y)$ is a periodic model potential and $\mathbf{A}(t)$ is the vector potential of the laser pulse. The configuration of the laser-solid interaction and the harmonic generation process is sketched in Fig. 1, in which the laser field is linearly polarized with an angle θ relative to the side of the crystal lattice.

One of the most important characteristics of a solid is its band structure [57,58], because it can greatly influence the electronic dynamics. In the two-dimensional case considered in the present work, one can introduce a rectangular unit cell with side lengths a_x and a_y . According to the Bloch theorem [59], in the velocity gauge description of the interaction given

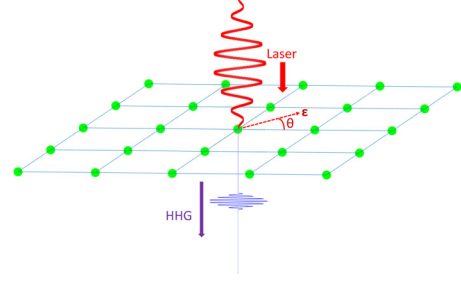


FIG. 1. Configuration of the laser-solid interaction. The laser is linearly polarized with an angle θ with respect to the lattice side. The generated harmonics can be detected behind the 2D material.

by Eq. (3), the wave function obeys the following conditions:

$$\Psi(x + a_x, y, t) = \Psi(x, y, t) e^{ik_x a_x}, \quad (4)$$

$$\Psi(x, y + a_y, t) = \Psi(x, y, t) e^{ik_y a_y}. \quad (5)$$

By separation of variables, one can thus introduce the following augmented plane-wave basis [56]

$$\psi_{n_x, n_y}(x, y) = \frac{1}{\sqrt{a_x a_y}} \exp(iK_x x + iK_y y), \quad (6)$$

in which the reciprocal lattice vector

$$K_x = \frac{2\pi}{a_x} n_x + k_x, \quad k_x \in \left[-\frac{\pi}{a_x}, \frac{\pi}{a_x} \right], \quad (7)$$

$$K_y = \frac{2\pi}{a_y} n_y + k_y, \quad k_y \in \left[-\frac{\pi}{a_y}, \frac{\pi}{a_y} \right], \quad (8)$$

where k_x and k_y are the crystal wave vectors in the first Brillouin zone of the reciprocal lattice, and n_x and n_y are integers. By using these basis states which satisfy the periodic conditions, an arbitrary time-dependent wave function can be expanded as

$$\Psi(x, y, t) = \sum C_{n_x, n_y}(t) \psi_{n_x, n_y}(x, y). \quad (9)$$

In the field-free case, $C_{n_x, n_y}(t)$ is of course time independent and one can diagonalize the corresponding field-free Hamiltonian to obtain the band structure [60]. Specifically, to get the band energy and the corresponding state of the 2D solid, one can solve the time-independent Schrödinger equation

$$H_{\text{free}} |\Psi\rangle = E |\Psi\rangle. \quad (10)$$

Inserting the expansion in Eq. (9) into the Schrödinger equation (10), we arrive at the following eigenvalue problem in terms of the expansion coefficients:

$$\sum_{n_x, n_y} \left\{ \delta_{m_x, n_x} \delta_{m_y, n_y} \frac{\hbar^2 \pi^2}{2m_0 a^2} \left[\left(2n_x + \frac{k_x a}{\pi} \right)^2 + \left(2n_y + \frac{k_y a}{\pi} \right)^2 \right] + V_{n_x, n_y, m_x, m_y} \right\} C_{n_x, n_y}^n = E^n C_{m_x, m_y}^n, \quad (11)$$

where n is an integer to index the energy. Note that, in the present work, we will consider a square cell with a lattice constant a , i.e., $a_x = a_y = a$.

To model the periodic potential of the 2D material, we adopt the well-known Kronig-Penney potential [61]. In a square unit cell extending from 0 to a along the lattice side, we introduce a

square well with a height of V_0 , which typically takes a negative value. The well extends from q_1 to q_2 in each direction, i.e.,

$$V(x,y) = \begin{cases} V_0, & \text{for } q_1 < x < q_2 \text{ and } q_1 < y < q_2, \\ 0, & \text{elsewhere.} \end{cases} \quad (12)$$

Therefore, the matrix elements for the potential term in Eq. (11) can be analytically evaluated by the following integrals:

$$V_{n_x n_y, m_x m_y} = \frac{V_0}{a^2} \int_{q_1}^{q_2} \int_{q_1}^{q_2} dx dy e^{i \frac{2\pi}{a} [(m_x - n_x)x + (m_y - n_y)y]}, \quad (13)$$

in which we take $V_0 = -0.15$ a.u., $q_1 = a/8$, and $q_2 = 7a/8$ in the present work.

With the availability of the matrix elements in Eq. (11), one can calculate the band energies of the 2D materials by repeatedly diagonalizing the Hamiltonian for different values of k_x and k_y in the first Brillouin zone.

For the time-dependent case where the laser field is present, one needs to evaluate the matrix elements of the interaction Hamiltonian H_{int} in Eq. (3). By the same expansion of Eq. (9), it is easy to show that the corresponding matrix elements

$$H_{n_x n_y, m_x m_y}^{\text{int}} = -\frac{\hbar e}{m_0} \left[\left(\frac{2\pi}{a} n_x + k_x \right) A_x(t) + \left(\frac{2\pi}{a} n_y + k_y \right) A_y(t) \right] \delta_{m_x n_x} \delta_{m_y n_y}, \quad (14)$$

where $A_x(t) = A(t) \cos \theta$ and $A_y(t) = A(t) \sin \theta$.

In all the results presented below, we choose an initial state calculated by diagonalizing Eq. (11) for $k_x = k_y = 0$ in the valence band. Please note that the choice of other crystal wave vectors in the first Brillouin zone as the initial state will lead to qualitatively similar conclusions. In fact, the total yield of each harmonic will be a sum of the contribution from every initial crystal vector.

Once the initial state is given, the TDSE given by Eq. (1) is propagated using the Crank-Nicolson (CN) method:

$$C_{n_x, n_y}(t + \Delta t) = \frac{1 - i(H_{\text{free}} + H_{\text{int}}) \frac{\Delta t}{2}}{1 + i(H_{\text{free}} + H_{\text{int}}) \frac{\Delta t}{2}} C_{n_x, n_y}(t), \quad (15)$$

where Δt is the time step. During the propagation of the wave function, the electronic current can be calculated at an arbitrary time:

$$\mathbf{j}(t) = -\frac{e}{m_0} [\langle \Psi(t) | \mathbf{p} | \Psi(t) \rangle]. \quad (16)$$

At the end of the interaction with the laser pulse, the harmonic generation spectrum can be computed through a Fourier transform to the current $\mathbf{j}(t)$, which is multiplied by a Hanning window [37] to improve the signal-to-noise ratio.

In all the results presented below, the laser pulse used has a \cos^2 envelope, i.e.,

$$\mathbf{A}(t) = A(t) \hat{\mathbf{e}} = A_0 \cos^2 \left(\frac{\pi}{T_d} t \right) \sin(\omega t) \hat{\mathbf{e}}, \quad (17)$$

where $\hat{\mathbf{e}}$ is the unit vector of the laser polarization, and $A_0 = E_0/\omega$ is the peak value of the vector potential with the peak electric field $E_0 = \sqrt{I_0/I_{\text{a.u.}}}$ (the atomic unit of laser intensity $I_{\text{a.u.}} = 3.51 \times 10^{16}$ W/cm²). For all the wavelengths

and intensities used below, we keep the number of optical cycles equal to 8, i.e., the pulse duration is $T_d = 16\pi/\omega$. Unless otherwise stated, the laser polarization $\hat{\mathbf{e}}$ is along the lattice side, i.e., $\theta = 0^\circ$.

III. RESULTS AND DISCUSSIONS

In this section, we will present our main numerical results. We will first present a comparison study of the band structure and harmonic spectrum between the 1D and 2D models. Then we will show the harmonic spectra of the 2D model at different laser parameters. By including a different number of basis sets in the expansion of Eq. (9), at specific laser conditions, we show that the conduction bands are excited by a ladder-climbing manner and they will lead to multiple-plateau structures in the harmonic spectrum. These features of the multiple-plateau structures are clearly seen when the electric field strength is gradually increased at different excitation laser wavelengths. Meanwhile, this is confirmed by a time-frequency analysis of the harmonic spectra at different polarization angles θ with respect to the side of the lattice. Finally, we present the orientation dependence of the harmonic spectra, which qualitatively agrees with recent experimental measurements.

A. Comparisons of 2D and 1D models

We first present the band structures of the 2D Kronig-Penney model in Fig. 2. In Fig. 2(a), the first three energy bands are shown in the whole (k_x, k_y) plane for the first Brillouin zone. As can be seen, there exist several critical points $\Gamma(0,0)$, $X(1,0)$, and $M(1,1)$.

In order to see clearly more energy bands which may be involved in the harmonic generation process, we show in Fig. 2(b) the first 50 bands along the direction of Γ -X, X-M, and M- Γ . Obviously, in the 2D case, the conduction bands are present as different clusters, which is different from the 1D case that will be shown later. We can label these clusters at the Γ critical point as (C1, C2, C3, ...). In each cluster, there are several energy bands staying very close. This will greatly enhance the transition probability under the interaction of a laser pulse since the laser electric field will change the electron momentum close to the boundary of the Brillouin zone, or to the nearly crossing points within the zone.

Before presenting the harmonic spectra for the 2D model, we show the comparison with the 1D Kronig-Penney model. In Fig. 3(a), we show the band structure of the 1D model, together with that of the 2D model along the Γ -X direction. As one can see, the band structures of the 2D model are more complicated than the 1D case. On the one hand, each corresponding energy band in the 1D evolves into a cluster of bands. On the other hand, there are new bunches of energy bands emerging between these clusters.

One expects that the great differences in the energy bands between the 1D and 2D models will reflect themselves in the harmonic spectrum. We show their spectra in Figs. 3(c) and 3(d) respectively under the same laser parameters, i.e., $\lambda = 3200$ nm and $I_0 = 0.436$ TW/cm². As one can see, the spectrum for the 2D model is more complicated and has a multiple-plateau structure and a higher cutoff energy than that in the 1D case. This can be qualitatively explained by their

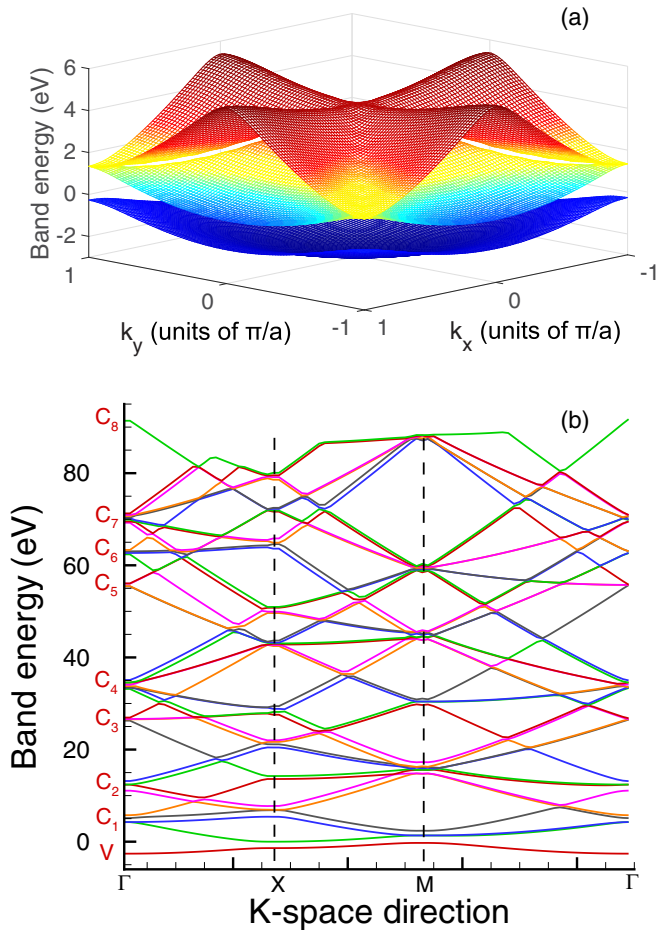


FIG. 2. The band structures for the 2D Kronig-Penney well. (a) is the full 3D representation for the first 3 energy bands. (b) shows the first 50 bands about the high-symmetry points indicated in the horizontal axis. Γ is the (0,0) point, X is the (1,0) point, M is the (1,1) point. The band clusters (C1, C2,...) have been marked in (b).

band structures. In the 1D model, the energy bands do not cross each other as shown in Fig. 3(a), thus the electron can only translate to a higher energy band at the boundary of the Brillouin zone. However, in the 2D case, energy bands may cross each other during the increase of the crystal momentum along the Γ -X direction, which means that for the same laser pulse the electron is much easier to be excited to higher energy bands than in the 1D case. This will lead to a higher photon energy and a multiple-plateau structure, which can be seen clearly in Fig. 3(d).

From the above comparison study, we can see that the harmonic generation dynamics in the 2D model is much more interesting and complex than the 1D model. In addition, one expects that the 2D model is more accurate in interpreting relevant experimental results in the 2D materials. For example, many properties of HHG, such as the orientation dependence and the influence of ellipticity of the laser polarization, can be qualitatively interpreted in the 2D model. Actually, when the beam of a laser pulse shines perpendicularly into a 3D solid material, the harmonic spectra detected mainly come from the interaction of the laser with the back surface of the material because of reabsorption inside the material [53]. Therefore, the

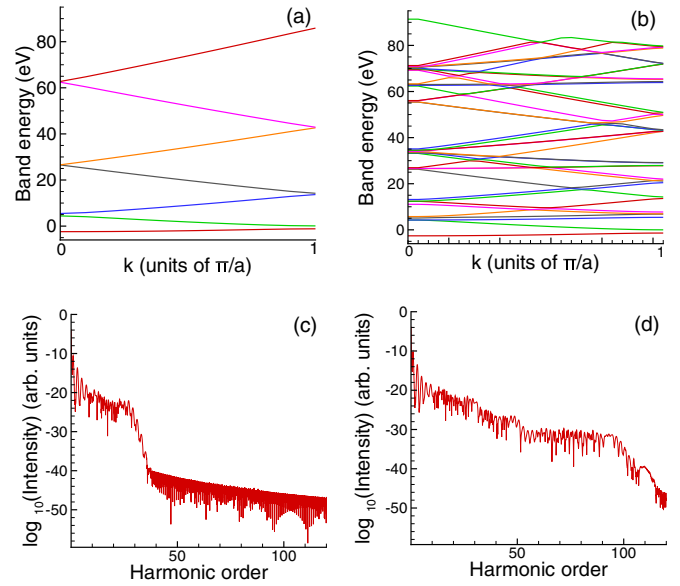


FIG. 3. Band structures for (a) the 1D model and for (b) the 2D model along the Γ -X direction. The corresponding harmonic spectrum is shown in (c) for the 1D and in (d) for the 2D model, generated by the same laser pulse of $\lambda = 3200$ nm and $I_0 = 0.436$ TW/cm².

2D model can in some extent simulate the harmonic generation of the back surface of the 3D material.

B. Harmonic spectra for the 2D case

Now we turn to investigate the harmonic generation spectra for our 2D model under different conditions and discuss their features and relationships to the band structures. We will see that, the excitations of the higher conduction bands proceed step by step and their involvements in the generation dynamics will lead to a multiple-plateau structure. First, this point can be confirmed by including a different number of basis states in the expansion of Eq. (9). Second, it can also be clearly seen from the harmonic spectra when one gradually increases the intensity of the laser pulse. Third, these features can be revealed by performing a time-frequency analysis for the harmonic signal at different laser polarization angles. As a distinct feature in the 2D case, the orientation dependence of the harmonic generation is theoretically studied, which qualitatively agrees with recent experimental studies.

1. Spectra calculated by using different number of basis states

We first consider the case where the polarization of the laser pulse is along the Γ -X direction. In Figs. 4(a) and 4(b), the harmonic spectra are respectively shown for the laser wavelength $\lambda = 1200$ nm and $\lambda = 3200$ nm at the same peak vector potential of $A_0 = 0.304$ a.u. As the initial state of the electron is at the critical point of Γ , we reproduce in Fig. 4(c) the band structure along the Γ -X direction. When the vector potential of the laser pulse becomes large enough, the momentum of the electron can be changed to be close to the crossing points along the Γ -X direction, two of which are indicated by dashed and solid vertical lines.

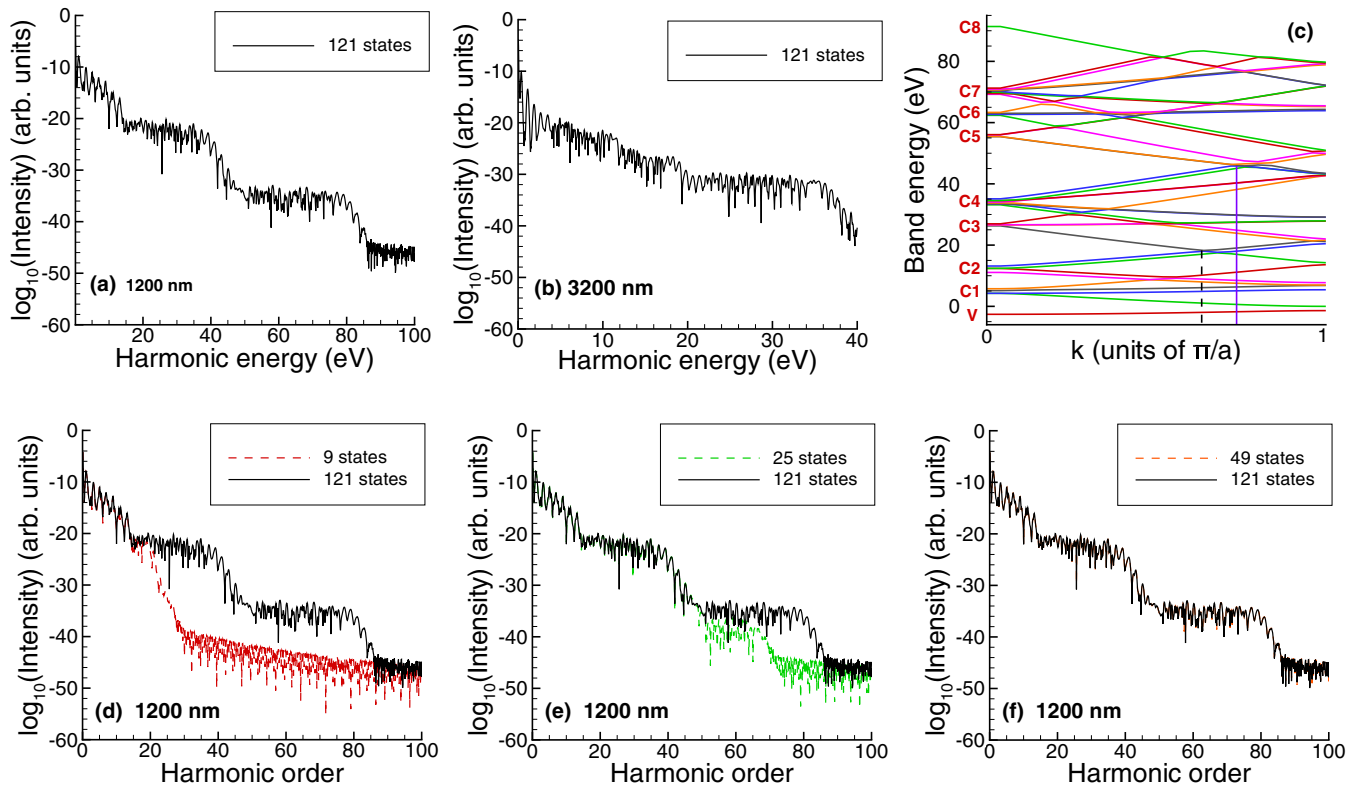


FIG. 4. HHG by different wavelengths of the laser pulse and by using different number of basis states for the 1200-nm case. Figures (a) and (b) respectively show the spectra for $\lambda = 1200$ and $\lambda = 3200$ nm at the same peak value of the vector potential. Figure (c) shows the band structure in the Γ -X direction. The two vertical lines indicate the two crossing points. Figures (d)–(f) show the resultant spectra for the case of $\lambda = 1200$ nm by using different number of basis states in the expansion (9).

In Fig. 4(a) when $\lambda = 1200$ nm, we can see two clear plateaus, with a cutoff energy close to 40 and 80 eV respectively. They come from the interband transitions from the band cluster (C3, C4) and (C5, C6, C7) to the valence band respectively. Following each of the two plateaus, the harmonic spectrum shows a sharp falling because of the large band gaps from C2 to C3 and from C4 to C5. Under the driving of the laser field, the electron can cross these gaps by a multiphoton excitation or a Zener-type tunneling.

One notices that there does not exist a clear plateau structure with a cutoff energy around 15 eV, corresponding to the transition between the cluster (C1, C2) to the valence band. This is probably because the photon energy of the 1200-nm laser is large (about 1 eV), so the spectrum in this region reflects a nature of the multiphoton process and this plateau is hard to be observed. To check this point, we increase the wavelength to 3200 nm (with a photon energy of 0.375 eV) but the peak value of the vector potential is kept the same. The resultant spectrum is shown in Fig. 4(b). In this case, one can clearly observe two plateaus with a cutoff energy around 10 and 17 eV respectively. They are caused by the transitions from the C2 and C3 to the valence band.

As one can see from the above results and discussions, for the 2D case, the transitions from the valence band to different conduction bands can proceed upward step by step via different crossing or mixing points in the band structures. This can actually be verified by including a different number of basis states in the expansion of Eq. (9) when one solves the TDSE.

In Figs. 4(d), 4(e) and 4(f), we show the result by including 9, 25, and 49 basis states, each compared with the converged result of the 121 basis states. In Fig. 4(d) we use 9 basis states, roughly corresponding to the lowest 9 energy bands, just the valence band, and C1, C2 conduction-band clusters. We can see that the HHG spectrum agrees well with the whole band HHG only at the low energy region ($0 \sim 15$ eV). However, the two obvious plateaus at larger photon energies have disappeared.

In Fig. 4(e), when we use 25 basis states, roughly corresponding to the lowest 25 energy bands, including the valence band, the C1 \sim C4 band clusters, and four other energy bands in the C5, the first plateau (20 \sim 39 eV) appears. The rightmost plateau still does not quite emerge in this spectral. As in our prediction, the second plateau is caused by the (C5, C6, C7) clusters. In Fig. 4(f) when we use 49 basis states, including the valence band and the (C1 \sim C7) band clusters, the HHG spectrum already overlaps with that of the 121 basis states. These simulations show that the HHG has a strong connection with the 2D energy band. Actually, we can get the conclusion that the interband transitions of different band clusters generate different plateaus in the HHG spectrum.

2. Spectrum variations against change of the laser intensity

In this part, we will investigate the dependence of the harmonic spectrum on the laser peak intensity. Since the amount of the electron's momentum change by the laser field is proportional to the vector potential of the field, we choose to

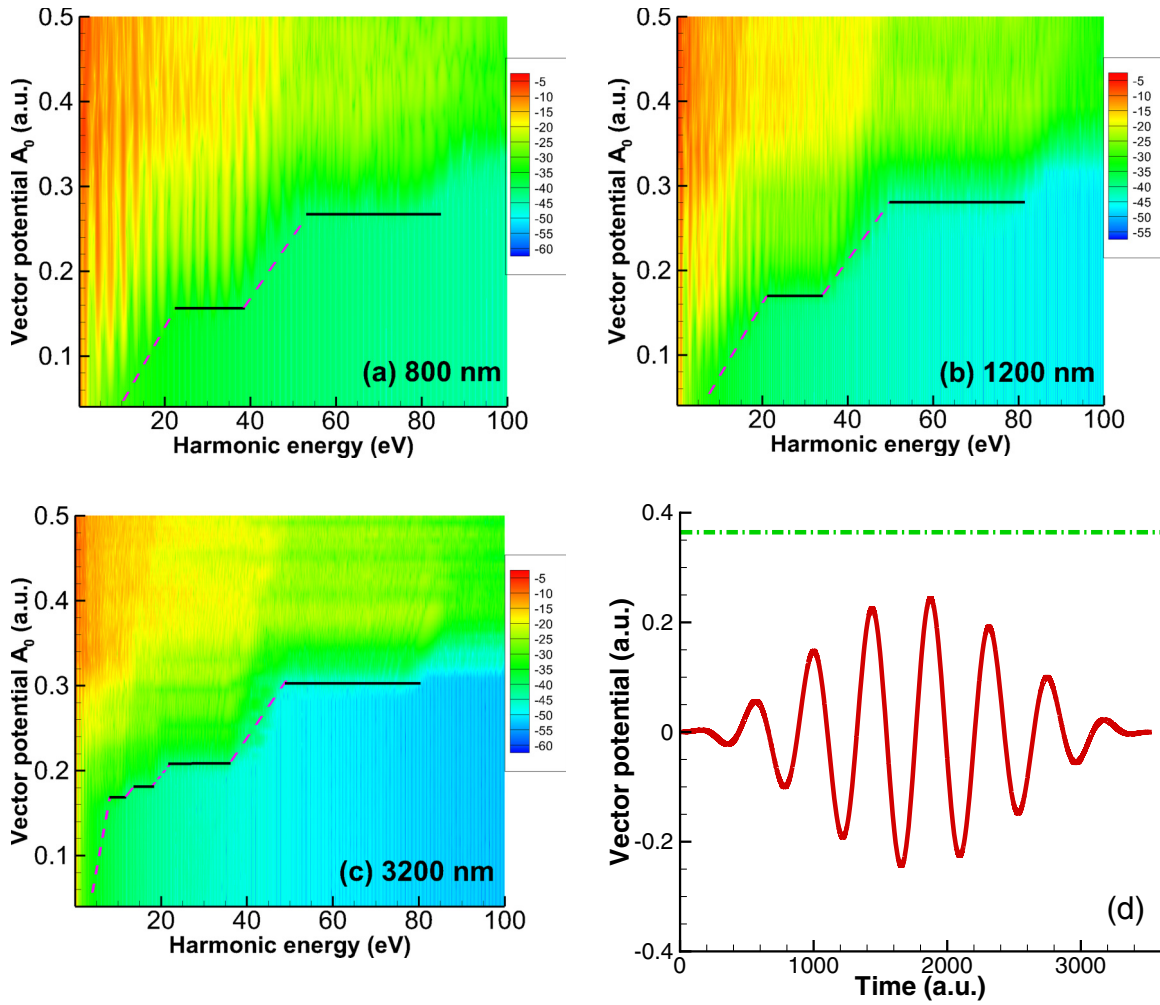


FIG. 5. Harmonic spectra as a function of electric field strength at different laser wavelengths: (a) $\lambda = 800$, (b) $\lambda = 1200$, and (c) $\lambda = 3200$ nm. (d) Vector potential of the electric field for the case in (c), in which the horizontal green dashed line represents the value of crystal momentum (0.365 a.u.) at the boundary of Brillouin zone.

plot the harmonic yield as a function of the peak value of the vector potential A_0 . In Figs. 5(a)–5(c), we present the variation of the harmonic yield for three different wavelengths, i.e., 800, 1200, and 3200 nm. Please note that, in all three cases, both the horizontal axis (harmonic energy) and vertical axis (vector potential) are taken to be in the same range.

As one can see, very clear stair-like structures are present in all of Figs. 5(a)–5(c). For guiding one’s eyes, we draw dashed lines and solid lines. The dashed lines indicate that the cutoff energy of each plateau is linearly proportional to the peak field strength of the laser pulse, which has previously been identified in the 1D case both from the two-band model and from the semiclassical analysis [37]. The linear relationship has also been experimentally verified [17]. Here, we focus on the black solid lines in Figs. 5(a)–5(c), which represent threshold laser intensities. One notices that horizontal solid lines are at similar values of vector potential for all three cases, which is understandable since the maximum change of the electron momentum is directly related to the peak value of the vector potential. When the electric strength of the laser reaches the threshold intensity, the electron is able to be excited to a higher conduction band cluster, whose subsequent transition back to

the valence band can form a new plateau in the harmonic spectrum.

It is worth pointing out that due to the existence of crossing points in the 2D band structure, it is unnecessary for the laser intensity to be so high that the change of the electron momentum can reach the boundary of Brillouin zone π/a . To see this clearly, let us examine the rightmost horizontal line in Fig. 5(c) with the wavelength $\lambda = 3200$ nm. We show the vector potential of the laser pulse in Fig. 5(d). One can see that the maximum vector potential is about 0.292 a.u., which is very close to the crossing point around 0.285 a.u. between the band cluster C4 and C5. On the contrary, the boundary of Brillouin zone π/a equals 0.365 a.u., as indicated by a black solid line in Fig. 5(d). This observation confirms that in the 2D case, the excitation of the conduction bands can proceed step by step via many of the crossing points in the 2D band structure, which is very different from the 1D case where the laser intensity often needs to be high enough for the electron to access the boundary of Brillouin zone. However, the above observation and analysis tells us the semiclassical picture of harmonic generation in the 1D model [41] is also qualitatively correct in the present 2D model.

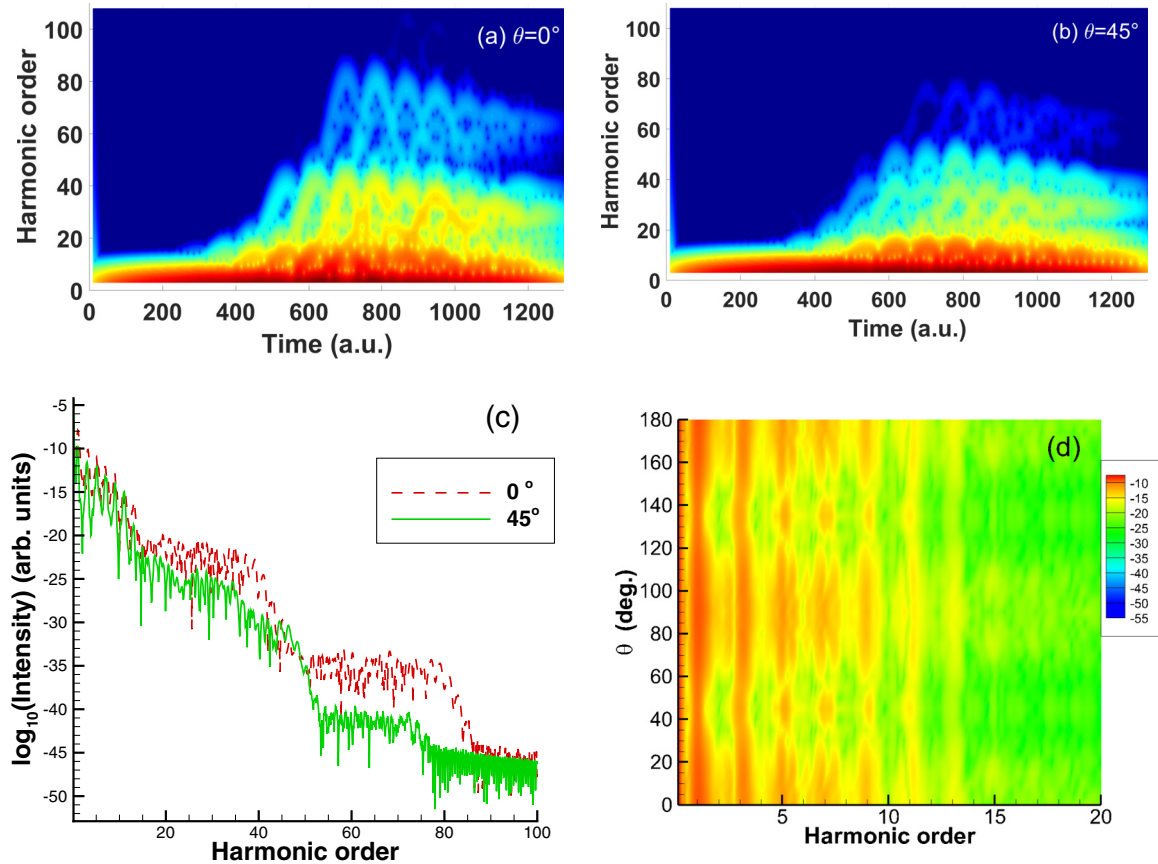


FIG. 6. Time-frequency analysis of the HHG and the orientation dependence of the HHG. (a) and (b) show the time-frequency spectrum at different angles $\theta = 0^\circ$ and $\theta = 45^\circ$. Figure (c) shows a yield comparison at these two angles and (d) shows the orientation dependence from 0° to 180° .

From these intensity-dependence studies, we clearly show that the harmonic spectrum is closely related to the energy band for the 2D material. Specifically, the interband transitions of different conduction-band clusters to the valence band produce different plateaus in the spectrum. The excitation by the external laser pulse of these conduction bands proceeds upward sequentially via different crossing points in the band structure.

3. Time-frequency analysis and orientation dependence of HHG

To further reveal the dynamics of harmonic generation and the formation of plateaus, we present a time-frequency analysis of the electronic current. As an example, we discuss the results for the wavelength $\lambda = 1200$ nm with a peak electric field $E = 0.012$ a.u. The maximum vector potential for this case equals about $0.83 \times (\pi/a)$. We show the time-frequency spectrographs at these laser parameters in Figs. 6(a) and 6(b) for the laser polarization $\theta = 0^\circ$ and 45° respectively. From these two panels, we can see the step-by-step structure clearly, which means that in the 2D model, the electron will first be excited in the lower band clusters and then gradually to higher band clusters as the time-dependent electric field strength is increased. In both cases, there are mainly three plateaus, each of which corresponds to the energy gap of the band clusters (C1, C2), (C3, C4), and (C5, C6, C7) with respect to the valence band.

However, when the laser polarization direction is changed from 0° to 45° , the details of the spectrographs look different. This is because the band structures are quite different in different directions. For example, the span of k from the critical point Γ to the boundary of the Brillouin is different for these two angles: π/a for 0° and $1.414 \times (\pi/a)$ for 45° . It means that it is harder for an electron to reach the boundary when $\theta = 45^\circ$. Therefore, from the comparison of the harmonic yield shown in Fig. 6(c), we can see the harmonic intensity for the 0° case is higher than that of the 45° case. The time-frequency analysis shows the intensity and structure differences due to the change of the energy band.

Finally, as mentioned above, an obvious feature for the 2D material is the orientation dependence of the harmonic spectra, which has been observed in recent experiments [17,18,20,21,53]. In Fig. 6(d), using our 2D model, we calculate the change of the harmonic spectrum as a function of the angle θ . Due to the four-fold symmetry in the energy band for our square lattice, as shown in Fig. 2(a), we find that the harmonic yield takes its maximum value at 0° (180°), and minimum at 35° (145°) and 55° (125°). Our results qualitatively agree with the experimental measurements [53]. However, we emphasize that the minimum is not at the angle of 45° (135°) simply because for our square structure in both the lattice space and momentum space, it is possible for the electron dynamics to happen between two sites on the diagonal

line with a lower probability due to a larger spacing than the sides of the lattice [17]. Actually, we confirm this by examining the angle distribution of the HHG at different laser intensities (results not shown here). Indeed, if one decreases the electric strength of the laser field, the peak structures around 45° (135°) will gradually disappear.

IV. CONCLUSIONS

In summary, we have presented theoretical studies on high-order harmonic generation from a 2D band structure. By analyzing the structures of the HHG spectra, we find the close relationship between harmonic generation and the band structures. The excitations of the higher conduction bands can proceed step by step when the laser intensity is increased, and multiple plateaus are identified in the spectra due to the transitions between different clusters of conduction bands to

the valence band. Most importantly, we show the distinct differences between the 1D and 2D models. On the one hand, the harmonic generation in 2D is critically dependent on the angle of the laser polarization with respect to the lattice side. On the other hand, because of the existence of many crossing points in the 2D band structures, it is much easier for the electron to be excited to higher bands at relatively lower laser intensities. Harmonic generation in the 2D band is contributed to by the mixing of these bands and shows multiple plateaus in the spectrum.

ACKNOWLEDGMENTS

This work is supported by the National Natural Science Foundation of China (NSFC) under Grants No. 11725416 and No. 11574010. L.Y.P. acknowledges the support by the National Science Fund for Distinguished Young Scholars.

-
- [1] A. McPherson, G. Gibson, H. Jara, U. Johann, T. S. Luk, I. A. McIntyre, K. Boyer, and C. K. Rhodes, *J. Opt. Soc. Am. B* **4**, 595 (1987).
 - [2] M. Ferray, A. L'Huillier, X. Li, L. A. Lompre, G. Mainfray, and C. Manus, *J. Phys. B* **21**, L31 (1988).
 - [3] M. Hentschel, R. Kienberger, C. Spielmann, G. Reider, N. Milosevic, T. Brabec, P. Corkum, U. Heinzmann, M. Drescher, and F. Krausz, *Nature* **414**, 509 (2001).
 - [4] P. M. Paul, E. S. Toma, P. Breger, G. Mullot, F. Augé, P. Balcou, H. G. Muller, and P. Agostini, *Science* **292**, 1689 (2001).
 - [5] P. B. Corkum and F. Krausz, *Nat. Phys.* **3**, 381 (2007).
 - [6] F. Krausz and M. Ivanov, *Rev. Mod. Phys.* **81**, 163 (2009).
 - [7] L.-Y. Peng, W.-C. Jiang, J.-W. Geng, W.-H. Xiong, and Q. Gong, *Phys. Rep.* **575**, 1 (2015).
 - [8] J. Itatani, J. Levesque, D. Zeidler, H. Niikura, H. Pepin, J. Kieffer, P. Corkum, and D. Villeneuve, *Nature* **432**, 867 (2004).
 - [9] S. Baker, J. Robinson, C. Haworth, H. Teng, R. Smith, C. Chirila, M. Lein, J. Tisch, and J. Marangos, *Science* **312**, 424 (2006).
 - [10] O. Smirnova, Y. Mairesse, S. Patchkovskii, N. Dudovich, D. Villeneuve, P. Corkum, and M. Y. Ivanov, *Nature* **460**, 972 (2009).
 - [11] H. J. Wörner, J. B. Bertrand, B. Fabre, J. Higuët, H. Ruf, A. Dubrouil, S. Patchkovskii, M. Spanner, Y. Mairesse, V. Blanchet, E. Mevel, E. Constant, P. B. Corkum, and D. M. Villeneuve, *Science* **334**, 208 (2011).
 - [12] K. A. Pronin, A. D. Bandrauk, and A. A. Ovchinnikov, *Phys. Rev. B* **50**, 3473 (1994).
 - [13] P. Kálmán and T. Brabec, *Phys. Rev. A* **52**, R21 (1995).
 - [14] P. Kálmán and T. Brabec, *Phys. Rev. A* **53**, 627 (1996).
 - [15] F. H. M. Faisal and J. Z. Kamiński, *Phys. Rev. A* **54**, R1769 (1996).
 - [16] O. E. Alon, V. Averbukh, and N. Moiseyev, *Phys. Rev. Lett.* **80**, 3743 (1998).
 - [17] S. Ghimire, A. D. DiChiara, E. Sistrunk, P. Agostini, L. F. Dimauro, and D. A. Reis, *Nat. Phys.* **7**, 138 (2011).
 - [18] O. Schubert, M. Hohenleutner, F. Langer, B. Urbaneck, C. Lange, U. Huttner, D. Golde, T. Meier, M. Kira, S. W. Koch, and R. Huber, *Nat. Photon.* **8**, 119 (2014).
 - [19] T. T. Luu, M. Garg, S. Yu. Kruchinin, A. Moulet, M. T. Hassan, and E. Goulielmakis, *Nature* **521**, 498 (2015).
 - [20] G. Ndabashimiye, S. Ghimire, M. Wu, D. A. Browne, K. J. Schafer, M. B. Gaarde, and D. A. Reis, *Nature* **534**, 520 (2016).
 - [21] Y. S. You, D. A. Reis, and S. Ghimire, *Nat. Phys.* **13**, 345 (2017).
 - [22] M. Siviš, M. Taucer, G. Vampa, K. Johnston, A. Staudte, A. Y. Naumov, D. M. Villeneuve, C. Ropers, and P. B. Corkum, *Science* **357**, 303 (2017).
 - [23] N. Yoshikawa, T. Tamaya, and K. Tanaka, *Science* **356**, 736 (2017).
 - [24] T. Higuchi, C. Heide, K. Ullmann, H. B. Weber, and P. Hommelhoff, *Nature* **550**, 224 (2017).
 - [25] L. A. Chizhova, F. Libisch, and J. Burgdörfer, *Phys. Rev. B* **95**, 085436 (2017).
 - [26] A. Schiffrin, T. Paasch-Colberg, N. Karpowicz, V. Apalkov, D. Gerster, S. Mühlbrandt, M. Korbman, J. Reichert, M. Schultze, S. Holzner, J. V. Barth, R. Kienberger, R. Ernstorfer, V. S. Yakovlev, M. I. Stockman, and F. Krausz, *Nature* **493**, 70 (2013).
 - [27] M. Schultze, E. M. Bothschafter, A. Sommer, S. Holzner, W. Schweinberger, M. Fiess, M. Hofstetter, R. Kienberger, V. Apalkov, V. S. Yakovlev, M. I. Stockman, and F. Krausz, *Nature* **493**, 75 (2013).
 - [28] G. Vampa, T. J. Hammond, N. Thiré, B. E. Schmidt, F. Légaré, C. R. McDonald, T. Brabec, D. D. Klug, and P. B. Corkum, *Phys. Rev. Lett.* **115**, 193603 (2015).
 - [29] G. Vampa, T. J. Hammond, N. Thiré, B. E. Schmidt, F. Légaré, C. R. McDonald, T. Brabec, and P. B. Corkum, *Nature* **522**, 462 (2015).
 - [30] M. Garg, M. Zhan, T. T. Luu, H. Lakhota, T. Klostermann, A. Guggenmos, and E. Goulielmakis, *Nature* **538**, 359 (2016).
 - [31] P. B. Corkum, *Phys. Rev. Lett.* **71**, 1994 (1993).
 - [32] M. Lewenstein, P. Salières, and A. L'Huillier, *Phys. Rev. A* **52**, 4747 (1995).
 - [33] P. Corkum, *Phys. Today* **64**, 36 (2011).
 - [34] O. D. Mücke, *Phys. Rev. B* **84**, 081202 (2011).
 - [35] S. Ghimire, A. D. DiChiara, E. Sistrunk, G. Ndabashimiye, U. B. Szafruga, A. Mohammad, P. Agostini, L. F. DiMauro, and D. A. Reis, *Phys. Rev. A* **85**, 043836 (2012).

- [36] G. Vampa, C. R. McDonald, G. Orlando, D. D. Klug, P. B. Corkum, and T. Brabec, *Phys. Rev. Lett.* **113**, 073901 (2014).
- [37] M. Wu, S. Ghimire, D. A. Reis, K. J. Schafer, and M. B. Gaarde, *Phys. Rev. A* **91**, 043839 (2015).
- [38] C. R. McDonald, G. Vampa, P. B. Corkum, and T. Brabec, *Phys. Rev. A* **92**, 033845 (2015).
- [39] G. Vampa, C. R. McDonald, G. Orlando, P. B. Corkum, and T. Brabec, *Phys. Rev. B* **91**, 064302 (2015).
- [40] P. G. Hawkins, M. Y. Ivanov, and V. S. Yakovlev, *Phys. Rev. A* **91**, 013405 (2015).
- [41] M. Wu, D. A. Browne, K. J. Schafer, and M. B. Gaarde, *Phys. Rev. A* **94**, 063403 (2016).
- [42] T. Tamaya, A. Ishikawa, T. Ogawa, and K. Tanaka, *Phys. Rev. Lett.* **116**, 016601 (2016).
- [43] T. Ikemachi, Y. Shinohara, T. Sato, J. Yumoto, M. Kuwata-Gonokami, and K. L. Ishikawa, *Phys. Rev. A* **95**, 043416 (2017).
- [44] C. R. McDonald, G. Vampa, P. B. Corkum, and T. Brabec, *Phys. Rev. Lett.* **118**, 173601 (2017).
- [45] Z. Guan, X. X. Zhou, and X. B. Bian, *Phys. Rev. A* **93**, 033852 (2016).
- [46] N. Tancogne-Dejean, O. D. Mücke, F. X. Kärtner, and A. Rubio, *Phys. Rev. Lett.* **118**, 087403 (2017).
- [47] N. Tancogne-Dejean, O. D. Muecke, F. X. Kaertner, and A. Rubio, *Nat. Commun.* **8**, 745 (2017).
- [48] K. K. Hansen, T. Deffge, and D. Bauer, *Phys. Rev. A* **96**, 053418 (2017).
- [49] N. Moiseyev, *Phys. Rev. A* **91**, 053811 (2015).
- [50] E. N. Osika, A. Chacón, L. Ortmann, N. Suárez, J. A. Pérez-Hernández, B. Szafran, M. F. Ciappina, F. Sols, A. S. Landsman, and M. Lewenstein, *Phys. Rev. X* **7**, 021017 (2017).
- [51] L. Liu, J. Zhao, W. Dong, J. Liu, Y. Huang, and Z. Zhao, *Phys. Rev. A* **96**, 053403 (2017).
- [52] S. Jiang, H. Wei, J. Chen, C. Yu, R. Lu, and C. D. Lin, *Phys. Rev. A* **96**, 053850 (2017).
- [53] H. Kim, S. Han, Y. W. Kim, S. Kim, and S. W. Kim, *ACS Photon.* **4**, 1627 (2017).
- [54] M. Wu, Y. You, S. Ghimire, D. A. Reis, D. A. Browne, K. J. Schafer, and M. B. Gaarde, *Phys. Rev. A* **96**, 063412 (2017).
- [55] L.-N. Li and F. He, *J. Opt. Soc. Am. B* **34**, 52 (2017).
- [56] J. Slater, *Phys. Rev.* **51**, 846 (1937).
- [57] M. S. Kushwaha, P. Halevi, G. Martínez, L. Dobrzynski, and B. Djafari-Rouhani, *Phys. Rev. B* **49**, 2313 (1994).
- [58] V. Kuzmiak and A. A. Maradudin, *Phys. Rev. B* **58**, 7230 (1998).
- [59] G. H. Wannier, *Elements of Solid State Theory* (Cambridge University, Cambridge England, 1960).
- [60] R. L. Pavelich and F. Marsiglio, *Am. J. Phys.* **84**, 924 (2016).
- [61] R. de L. Kronig and W. G. Penney, *Proc. R. Soc. A* **130**, 499 (1931).